JPG Journal of Petroleum Geology www.jpg.co.uk

Journal of Petroleum Geology, Vol. 40(1), January 2017, pp 105 - 118

RESERVOIR POTENTIAL OF DEEP-WATER LACUSTRINE DELTA-FRONT SANDSTONES IN THE UPPER TRIASSIC YANCHANG FORMATION, WESTERN ORDOS BASIN, CHINA

Shengli Li[1*], Y. Zee Ma[2], Xinghe Yu[1] and Shunli Li[1]

This paper investigates the reservoir characteristics of deep-water lacustrine-delta sandstones in the Upper Triassic Yanchang Formation in the western Ordos Basin, north-central China. The Yanchang Formation has previously been interpreted as a shallow-water lacustrine deltaic succession, and this interpretation has been used to guide petroleum exploration activities which have however met with only limited success. The present study integrates thin-section, wireline log, X-ray diffraction and SEM data from wells in the western Ordos Basin to determine the sedimentary and diagenetic characteristics of sandstones in the C6 and C4+5 sub-members of the Yanchang Formation, and to interpret the units' depositional environment.

The C6 and C4+5 sub-members in the study area are composed of: mudstones and fine-grained sandstones, which are interpreted as deep-water pro-delta deposits; laterally-extensive sand sheets (outer delta-front deposits); and small-scale distributary channel and mouth bar sandbodies (inner delta-front deposits). The sandstones have reservoir potential but diagenesis has had a range of effects on reservoir quality. Compaction together with cementation by calcite and clay minerals including chlorite and kaolinite may have affected pore throat geometry and permeability adversely. However dissolution of feldspars and calcite cement created secondary porosity. Hydrocarbon accumulations may occur in delta-front channel and mouth bar sandbodies. Core studies show that some sandstone intervals have relatively good reservoir properties with porosity up to 15% and permeability up to 9mD.

INTRODUCTION

Although numerous studies have investigated deep-marine clastic systems and shallow-water lacustrine deltas, studies of lacustrine deltas developed under deep-water conditions are less common. In lacustrine basins, changes in lake-level are generally smaller in magnitude than changes of eustatic sea level but may still influence patterns of deltaic sedimentation (e.g. Kasse, 2014; Du, 2014; Xiao *et al.*, 2013; Han, *et al.*, 2009). In previous studies of large-scale non-marine basins in China (Yao *et al.*.1995; Zou *et al.,* 2008; Zhu and Tao, 2008), lacustrine deltas were in general interpreted as having developed in shallow-

[1]School of Energy Resources, China University of Geosciences, Beijing, China.
[2] Schlumberger, 1675 Broadway, Suite 900, Denver, CO 80202, USA.
*corresponding author, email: slli@cugb.edu.cn

Key words: Deep-water lacustrine delta, delta front deposits, Triassic, Yanchang Formation, Ordos Basin, sandstone diagenesis, secondary porosity.

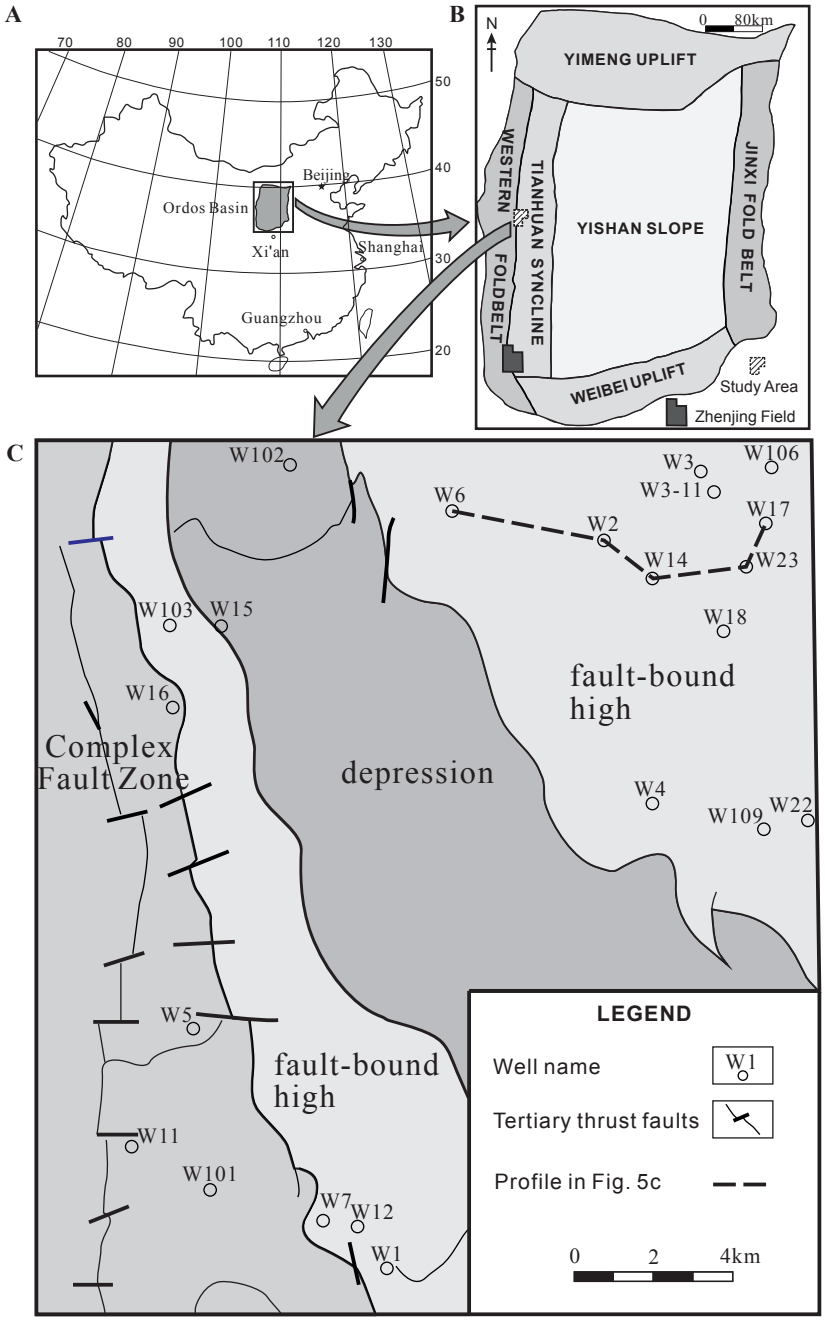

Fig. 1. The main map (Fig. 1C) shows the location of the study area in the western Ordos Basin, north-central China (see Figs 1A, B), and the locations of the wells studied. The dashed line in Fig. 1C indicates the line of profile of the section in Fig. 5C.

water settings, and this interpretation has been used to provide a framework for hydrocarbon exploration (Han *et al.,* 2009; Yu *et al.,* 2009; Liu *et al.,* 2012). In the Ordos Basin, north-central China (Fig. 1), thick sandstones and shales in the Upper Triassic Yanchang Formation have in general been interpreted as the deposits of a shallow-water lacustrine delta (Wu *et al.,* 2004; Zou *et al.,* 2008; Han *et al.,* 2009). The present study however suggests that in the western part of the basin, certain intervals such as the C4+5 and C6 sub-members were deposited in a deep-water delta-front setting, with maximum water depths of ca. 150 m (Yuan *et al.,* 2015). Evidence for this includes the presence of delta-front mouth bar sandstones which in general are not well-developed in shallow-water lacustrine deltas (Yu *et al.,* 2009; Liu *et al.,* 2012), and the occurrence of abundant mud-rich fine-grained sandstones and laminated mudstones wich are interpreted as relatively deep-water deposits (Guo *et al.,* 2008; Yuan *et al.,* 2015).

Economic accumulations of hydrocarbons in the western Ordos Basin are present in the Jurassic Yan'an Formation which overlies the Yanchang Formation (Johnson *et al.,* 1989). Although the Yan'an Formation is the main oil-producing interval (Lei and Zhang, 1998; Zheng, 2012), the Yanchang Formation has been the target of recent exploration in the study area; thus 6.5 tons of oil were produced during well tests from well W103 (location in Fig. 1C) from an interval between 2728.5 and 2731.5 m depth.

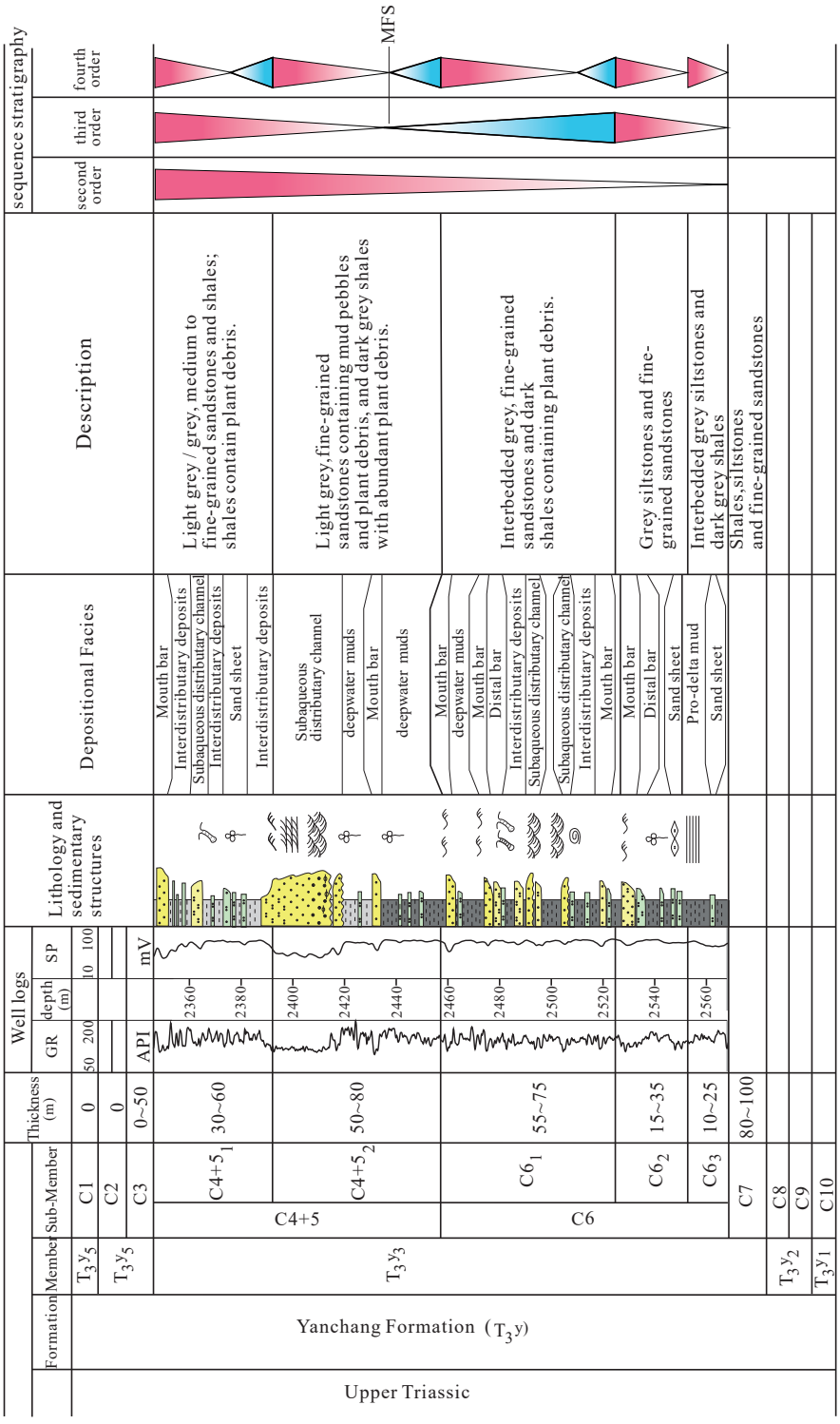

Fig. 2. Sequence stratigraphy and sedimentary facies of the Upper Triassic succession in the study area. The Yanchang Formation (228-199.6 Ma) is divided into five members (T_3y_{1-5}) and ten sub-members (C1 to C10). Sub-members C4+5 and C6, the focus of this paper, together comprise two third-order sequences (Zhao *et al.*, 2010) (sequence definition after Slatt, 2006).

However in general exploration results have been disappointing and no significant commercial volumes of hydrocarbons have so far been discovered in the Yanchang Formation. An improved understanding of the depositional and diagenetic characteristics of the sandstones in this formation may help to explain this lack of exploration success.

Primary porosity has been significantly reduced in sandstone intervals in the Yanchang Formation in the study area as a result of compaction and clay mineral and calcite cementation (Luo *et al.,* 2009). However, core and thin section analyses suggest that secondary porosity was created during diagenesis and may locally have improved the sandstones' reservoir qualities.

The aim of this paper is therefore to investigate the sedimentary characteristics of deep-water lacustrine delta-front sandstones in the Yanchang Formation in the western Ordos Basin, and to assess the impact of depositional and diagenetic processes on the sandstones' reservoir properties.

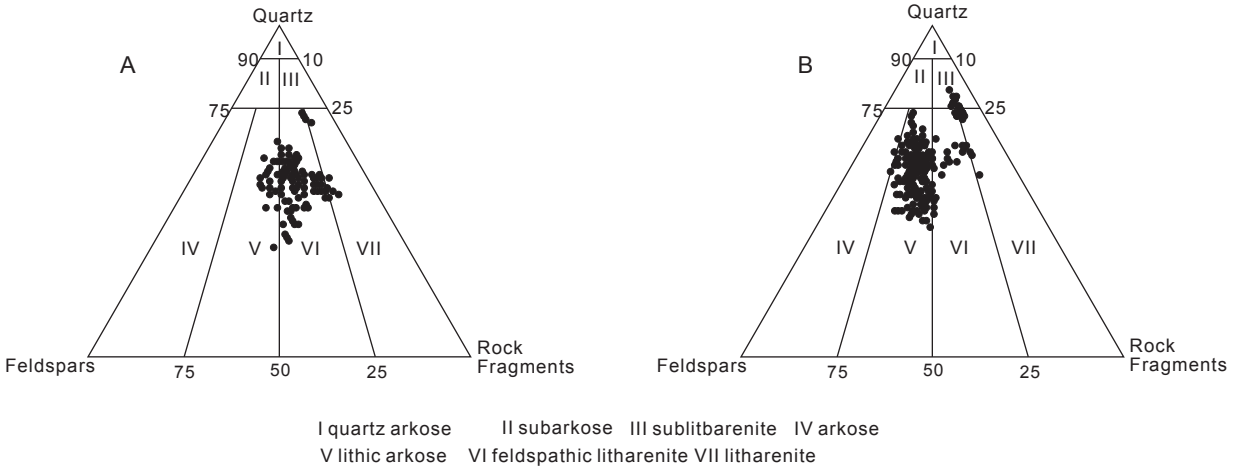

Fig. 3. Compositional classification of (A) the C4+5 sandstones and (B) the C6 sandstones of the Yanchang Formation in wells in the study area. The triangular plots show that the sub-members are dominated respectively by feldspathic litharenites and lithic arkoses, and that the sandstones in the C6 sub-member are compositionally more mature than those in the C4+5.

Geological setting

The intracratonic Ordos Basin in north-central China (Li *et al.,* 2009; Yang *et al.,* 2007; Wang and Al-Aasm, 2002) is composed of a number of first-order structural units: the Yimeng and Weibei uplifts, the Jinxi foldbelt, the Yishan slope, the Tianhuan syncline, and an unnamed western fold-and-thrust belt (Yang *et al.,* 2005) (Fig. 1). This study focuses on an area in the western Ordos Basin located between the Tianhuan syncline and the western fold-and-thrust belt (Figs 1B and 1C).

In the study area, the lacustrine Upper Triassic Yanchang Formation (228 to 199.6 Ma) is unconformably overlain by the coal-bearing Lower Jurassic Yan'an Formation (Johnson *et al.,* 1989), and rests disconformably on the Zhifang Formation (Zeng and Li, 2009). The Yanchang Formation contains high-TOC (>2.0%) oil-prone shale source rocks together with sandstones with reservoir potential (Hanson *et al.,* 2007; Wang *et al.,* 2010; Luo *et al.,* 2006, 2009). The formation is widely distributed throughout the Ordos Basin and has a thickness ranging from 184 to 2060 m (Wang *et al.,* 2010), and in general dips towards the SW as a result of basin-scale structural tilting. Clastic materials in the formation was transported from sediment provenance areas to the north, west and SW which were dominated by schists and gneisses (1.7–2.1 Ga and 2.3–2.6 Ga, respectively) together with marine sandstones and carbonates (250-500 Ma) (Wei *et al.,* 2003; Xie and Heller, 2013).

The Ordos Basin evolved from an intracratonic basin to a rift depression as a result of late Indosinian tectonism during the Late Triassic (Darby *et al.*, 2002; Yue *et al*., 1998) with a change from mainly open-marine to mainly non-marine deposition (Hu *et al*., 2013). The western Ordos Basin was dominated by fluvio-lacustrine and deltaic environments (Wu *et al.,* 2004), and the Zhenbei-Jingchan palaeo river formed a large-scale lacustrine delta system (covering > 2000 km^2) at the basin margin. The study area for this paper is located in the distal portion (i.e. the east) of this deltaic system.

Based on variations in lithology as indicated by wireline log response, the Yanchang Formation can be divided into five members ($T_3y_1 - T_3y_5$) and ten sub-members referred to as C1 to C10 from top to bottom (Fig. 2) (Zhao *et al.,* 2010; Wang *et al.,* 2009). This study focuses on the C4+5 and C6 sub-members.

Wang *et al.* (2008) used well-log data to determine the water depths in which the Yanchang Formation was deposited and recognized three deep-water intervals: C9, C7 and C4+5 (Fig. 2). The C6 sub-member was deposited in a delta-front setting which deepened abruptly before the deposition of the C4+5 sub-member. A third-order maximum flooding surface (MFS) can be inferred from the presence of dark grey shales with high gamma-ray (GR) log readings in the lower part of the C4+5 sub-member (referred to as C4+5$_2$) (Fig. 2).

MATERIALS AND METHODS

This study is based on cores, thin sections and wireline logs from an area covering about 420 sq. km in the west-central Ordos Basin (Fig. 1). Twenty-two wells with wireline logs were investigated (Fig. 1C), of which nineteen were cored and more than 650 m of core was analysed in detail. Thin sections were prepared from 309 core samples from eight wells (W2, W3, W4, W5, W14, W17, W103 and W109: Fig. 1C). Lithologies, sedimentary structures, porosity, and permeability were analysed or measured from cores or core samples. Depositional environments were interpreted from cores and wireline logs.

Sandstone diagenesis was investigated from the analysis of 46 thin sections of the Yanchang Formation

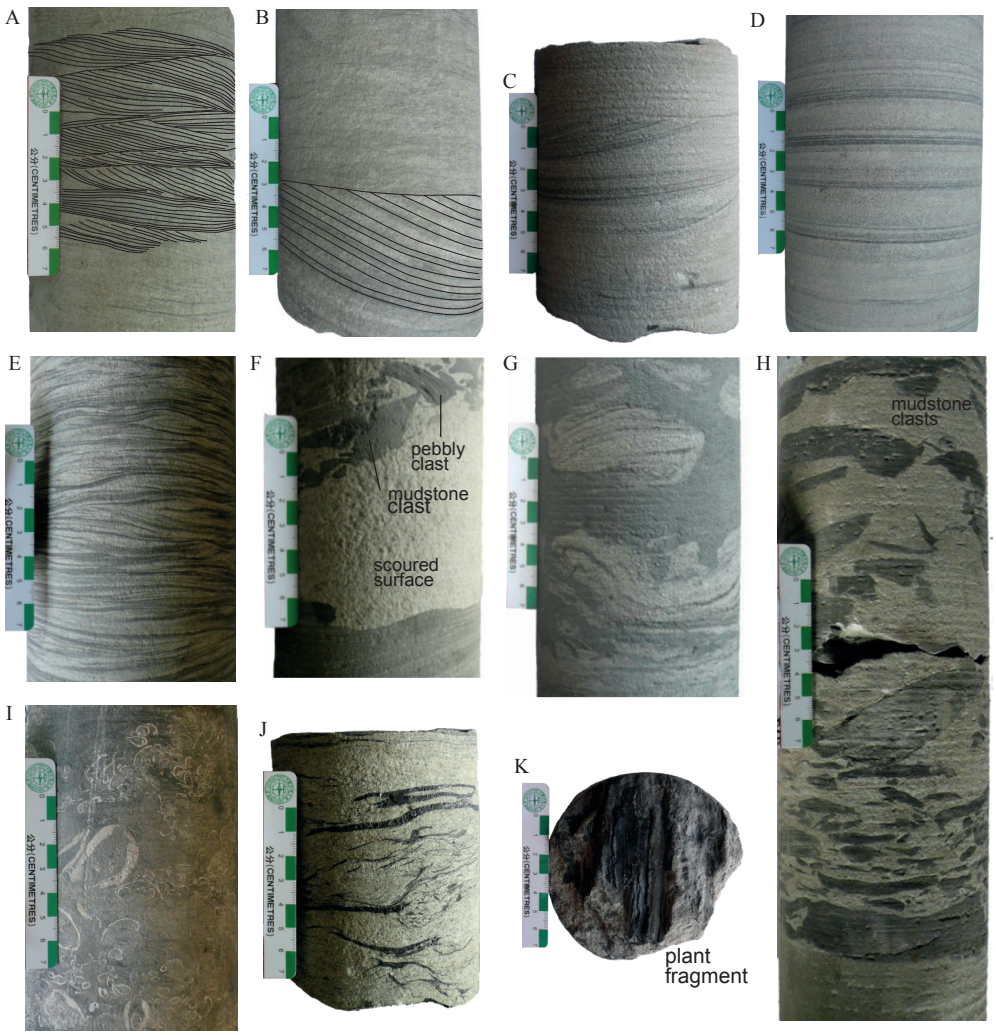

Fig. 4. Core photographs showing sedimentary structures in Yanchang Formation sandstones, siltstones and mudstones in the C6 and C4+5 sub-members in the study area. (A) Trough cross-stratification, often recorded at the base of channel sandbodies; (B) planar cross-stratification which often occurs in cores above trough cross-stratification; (C) trough and planar cross-stratification, interpreted to indicate lateral channel accretion; (D) parallel lamination in channel sandstones; (E) wave ripple cross-lamination, interpreted to occur in delta-front sandstones; (F) scoured surface at the base of a channel sand; the overlying section includes mudstone rip-up clasts; (G) deformation due to soft-sediment slumping; (H) oriented mudstone rip-up clasts indicating palaeoflow direction; (I) pelecypods in delta front or pro-delta siltstones; (J, K) coal lenses and plant fragments indicating a delta plain or inner delta-front setting.

from the eight wells identified above. X-ray diffraction analysis was used to investigate the authigenic clay minerals in fine-grained samples (grain size <2μm) from five wells (W3, W5, W14, W17, W109), together with scanning electron microscope studies of samples from well W17 in the NE of the study area (Fig. 1C). Porosity and permeability data were obtained from the 309 core samples; this data was provided by the Huabei Branch Company of SINOPEC, Zhengzhou.

SEDIMENTARY CHARACTERISTICS OF THE YANCHANG FORMATION

The C4+5 and C6 sub-members of the Yanchang Formation have present-day burial depths of 2180 – 2650 m, and in general consist of mudstones, siltstones and fine- to medium-grained sandstones. Sandstones in the C4+5 sub-member are dominated by feldspathic litharenites and lithic arkoses (Fig. 3A) with 33-74% quartz, 6-35% feldspar (K-feldspar and plagioclase), and 16–41% rock fragments (igneous, sedimentary and metamorphic). The moderate sorting and predominace of sub-angular grains indicate moderate textural maturity. The C6 sandstones are dominated by lithic arkoses with subordinate feldspathic litharenites and sub-litharenites (Fig. 3B). Quartz represents 39–81%, feldspar 3–38% and lithic fragments (mainly metamorphic debris) 8–35% of the samples. Textural maturity and sorting are moderate, and grains are mainly sub-angular with some sub-rounded.

In general, mean grain size decreases upwards from the C6 sub-member to the MFS in the lowermost part of the C4+5 interval (Fig. 2). Above, grain size increases and sandstone intervals become thicker. The upward

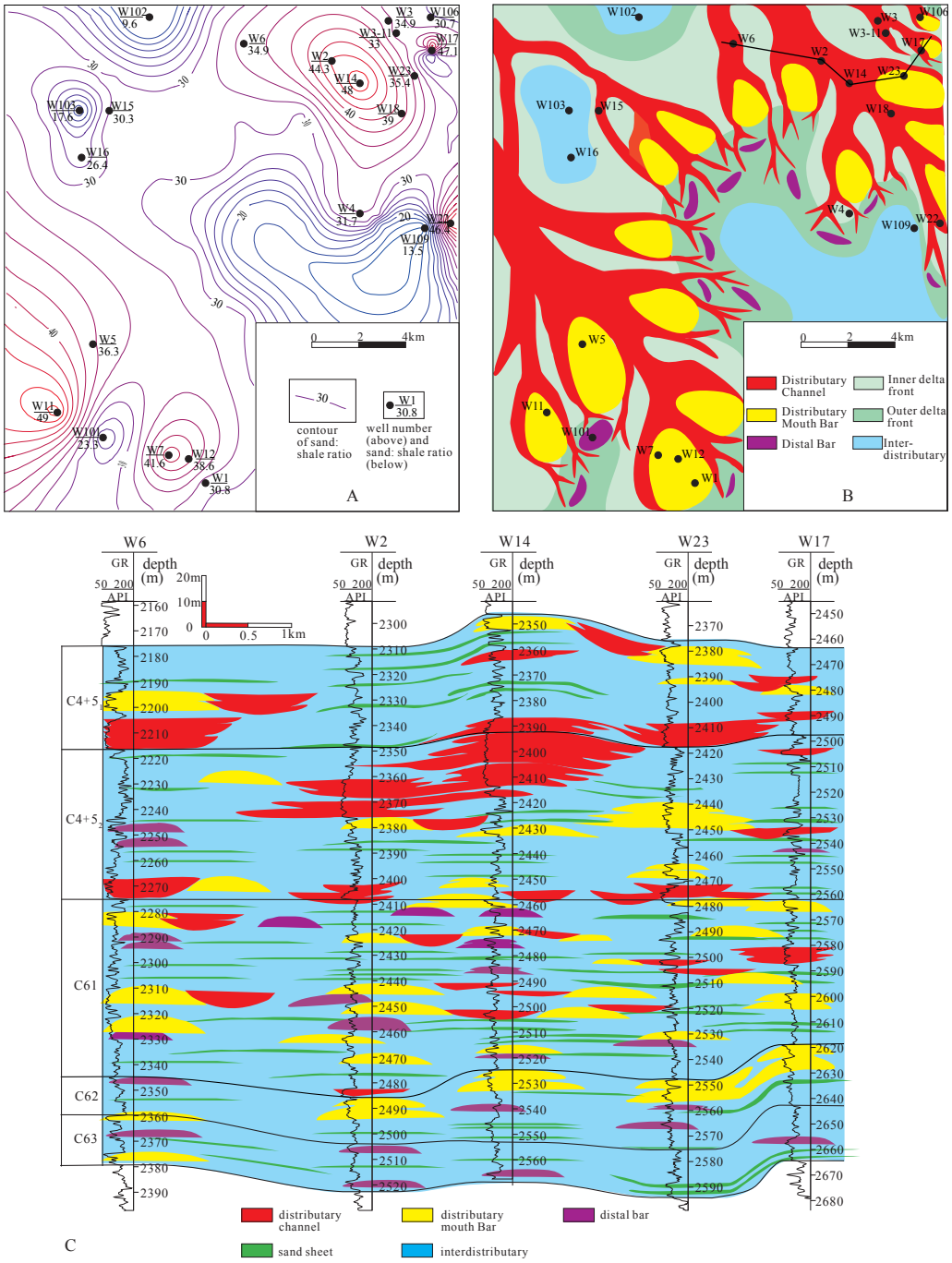

Fig. 5. (A) Map of the study area showing contours of the sand:shale ratio in the C4+5$_2$ interval; the contours were controlled by well data and were interpolated at inter-well locations using a kriging method. (B) Depositional facies distribution of the C4+5$_2$ interval in the study area. (C) Correlation of sedimentary facies along a west-east profile between wells W6 and W17 (profile location in Fig. 5B).

increase in grain size and sand: shale ratio indicates overall progradation.

Depositional features observed in cores of the studied intervals include trough cross-stratification, tabular cross-stratification and parallel lamination in fine- and medium-grained sandstones and mudstones (Fig. 4). In general, small-scale trough cross-stratification occurs in the lower parts of sandbodies interpreted as channel fills (Fig. 4A). At the base of these sandbodies are erosive surfaces (Fig. 4F) with rip-up clasts (Fig. 4H). Tabular cross-stratification (Figs 4B and 4C) and parallel lamination (Fig. 4D) were observed and may be present within a single sandbody or as part of a fining-upward sequence that suggests waning channel flow during sediment deposition. Small-scale current ripples, wave ripples and lenticular lamination were present in silty sandstones and mud-rich siltstones (Fig. 4E) and suggest deposition in ddistal bars and sand sheets. Syndepositional deformation structures (Fig. 4G) were recorded in some mud-rich sandstones. Although fossils were not abundant in the C4+5 and C6 sub-members, foraminifera and pelecypods were

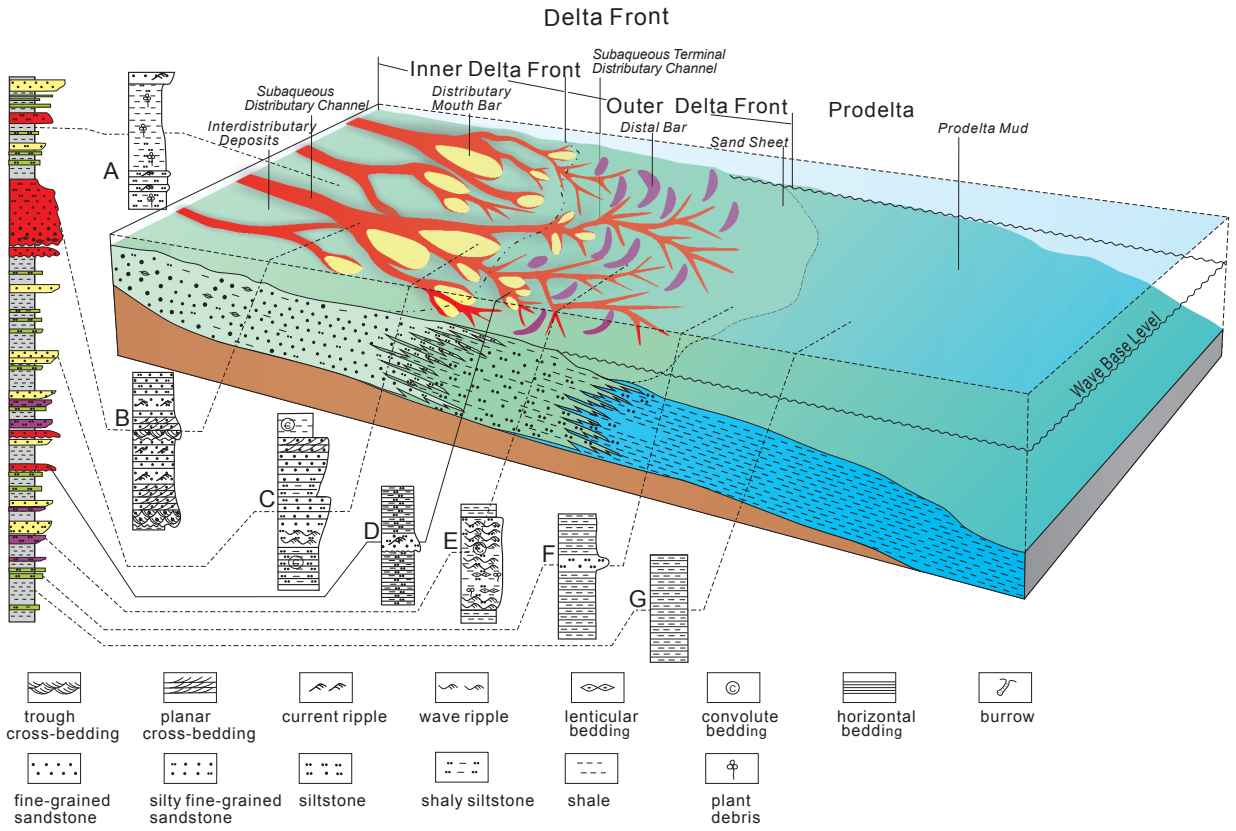

Fig. 6. Block diagram showing a generalised depositional model for a lacustrine delta front, divided into proximal and distal sectors, in front of which is the mud-rich pro-delta.
A: interdistributary fines; B: sub-aqueous distributary channel sands; C: mouth bar sands; D. terminal distributary channel sands; E. distal bar sands; F. distal sand sheet; G. pro-delta muds.

recorded in mudstone-rich intervals (Fig. 4I) together with woody debris and plant fragments (Figs 4J and 4K) whose presence increases upwards. Coal intervals and bioturbation were occasionally observed.

The C4+5 sub-member was deposited in maximum water depths of ca. 150 m (Yuan *et al.*, 2015). The occurrence of dark-grey laminated mudstones and siltstones in these units in the study area (Fig. 2) suggests low-energy deep-water settings. The distal part of the delta front was located in the far east of a deltaic system dominated by fine- to medium-grained sandstones, with small-scale sedimentary structures observed in cores (Fig. 4). The C4+5 and C6 sub-members in the study area are therefore interpreted as relatively deep-water delta-front deposits.

Depostional facies and facies distribution

Five depositional facies in the C6 and C4+5 sub-members of the Yanchang Formation in the study area were interpreted from wireline logs and lithological observations (cf. Coleman, 1982): distributary channel, distributary mouth bar, interdistributary, distal bar, and sand sheet.

An attempt was made to predict the facies distribution in the study area at inter-well locations and at locations where no wireline logs were available. First, the sand: shale ratio of the C4+5$_2$ interval was determined from well log interpretations from the 22 wells investigated (Fig. 5A). The ratio is in general <50% and exceeds 40% at only a few well locations. Then, a contoured map of the sand: shale ratio in the C4+5$_2$ unit was prepared (Fig. 5A) using a kriging interpolation method. By integrating the map of sand-shale ratio (Fig. 5A) with the depofacies characteristics interpreted from well logs, a map of facies distributions in the study area was constructed (Fig. 5B).

A section between wells W6 and W17 in the north of the study area (Fig. 5C) shows that potential sandstone reservoir units in the C4+5 and C6 sub-members are present at depths of between 2180 m (well W6) and 2650 m (well W17, Fig. 5C). These units could be correlated between wells (Fig. 5C) and interpolated at inter-well locations.

Areas with relatively high sand: shale ratios were identified in the NE and SW of the study area (Fig. 5A). The facies map (Fig. 5B) suggests that sandstones in these areas are mainly distributary channel and mouth bar deposits, and sandbodies are of relatively small scale with widths <3km and lengths <4 km. More laterally-extensive sand sheets are also present (Fig. 5C) and are typical of unconfined outer delta-front deposits (Fig. 5B).

Table 1. Average reservoir properties (porosity and permeability) of the C4+5 and C6 sandstones in the study area. Data from 309 samples from eight wells (W2, W3, W4, W5, W14, W17, W103 and W109). Sample depths between 2180m and 2650m.

	Porosity (%)					Permeability (mD)				
Layer	$C4+5_1$	$C4+5_2$	$C6_1$	$C6_2$	$C6_3$	$C4+5_1$	$C4+5_2$	$C6_1$	$C6_2$	$C6_3$
Average	12.4	9.6	8.9	5.7		1.61	0.48	0.37	0.2	
Maximum	13.5	13.6	15.3	10	No data	9.91	1.72	3.05	1	No data
Minimum	10.9	2.2	1.5	2.9		0.19	0.07	0.05	0.06	
Sample count	10	83	202	14		10	83	202	14	

Table 2. Relative contents of clay minerals in the C4+5 and C6 sandstones. Data are from X-ray diffraction analysis of samples from wells W3, W5, W14, W17 and W109 (locations in Fig. 1C); sample number = 50. Sample depths between 2393m and 2575m.

Sub-member		Clay mineral content			Illite/smectite (I/S) %
		Illite (I) %	Kaolinite (K) %	Chlorite (C) %	
C4+5	Average	16.02	27.7	44.4	11.9
	Range	10 - 23	24 - 32	38 - 49	8 - 14
C6	Average	12.3	23.5	55.5	8.7
	Range	6 - 22	14 - 29	41 - 60	5 - 15

The facies distribution pattern is consistent with the model that the C4+5 and C6 sub-members of the Yanchang Formation were in general deposited in a deep-water lacustrine delta-front system (Fig. 6). Sandstones with reservoir potential were deposited in distributary channels and mouth bars. Relatively large-scale channel sandstones occur more frequently in the upper part of the C4+5 sub-member than in the C6 (Fig. 5C).

Depositional Model

A model of deep-water lacustrine delta-front deposition for the C4+5 and C6 sub-members was constructed (Fig. 6) based on the facies distribution (Fig. 5B) and well correlations (Fig. 5C), and in the context of previous studies (Zou *et al.*, 2008; Zhu *et al*., 2013). The inner (proximal) portion of the delta front is dominated by distributary channels and mouth bars; the distal portion by terminal distributary channels, distal bars and sheet sands. Fine-grained and muddy deposits occur in the pro-delta region.

Facies in the inner delta front include subaqueous interdistributary deposits (Fig. 6,A), amalgamated multicycle distributary channel sands (Fig. 6,B), and amalgamated multicycle mouth bar sands (Fig. 6,C). Facies in the distal portion of the delta front include distal bar sands (Fig. 6, E) and sand sheets (Fig. 6, F), together with deep-water shales and thin, fine-grained or silty sandstones (Fig. 6, G) which are often interbedded due to high-frequency progradational and retrogradational cycles. Although no TOC data is available in the study area, in the nearby Zhenjing oilfield (location in Fig. 1B), ten samples from the C4+5 interval and 31 samples of pro-delta muds from the C6 interval had average TOC contents of ca. 2.8% and 1.4%, respectively, suggesting that similar mudstones in the study area may have source rock potential where organic rich.

In lacustrine settings, deltaic facies zones are influenced by the overall lake level. With high lake levels, deep-water lacustrine deltas develop with a wide delta front and a narrow delta plain. Coarse-grained deposition occurs in the proximal delta front with the formation of multicycle distributary channels and mouth bars, together with finer-grained and muddy sediments in more distal settings. With low lake levels, a shallow-water delta develops and is dominated by deposition on the the delta plain (Zou *et al.,* 2008; Zhu, 2008). Subaerial distributaries or subaqueous channels may erode earlier distributary mouth bars, which are consequently less likely to be preserved.

DIAGENESIS

Compaction, pressure solution and cementation

Compaction results in most porosity loss in sandstones, especially in fine-grained sandstones (Shou *et al.,* 2003). Potential reservoir units in the C4+5 and C6 sub-members consist of fine-grained sandstones and siltstones (Fig. 7A) deposited in distal delta-front settings, which have undergone significant compaction. The C6 sandstones have lower average porosity and permeability values than the overlying C4+5 sandstones in the eight wells studied (Table 1).

In a normally-pressured section, porosity is reduced with depth due to compaction and diagenetic changes such as dissolution and cementation. In the Yanchang Formation sandstones studied, pressure solution has

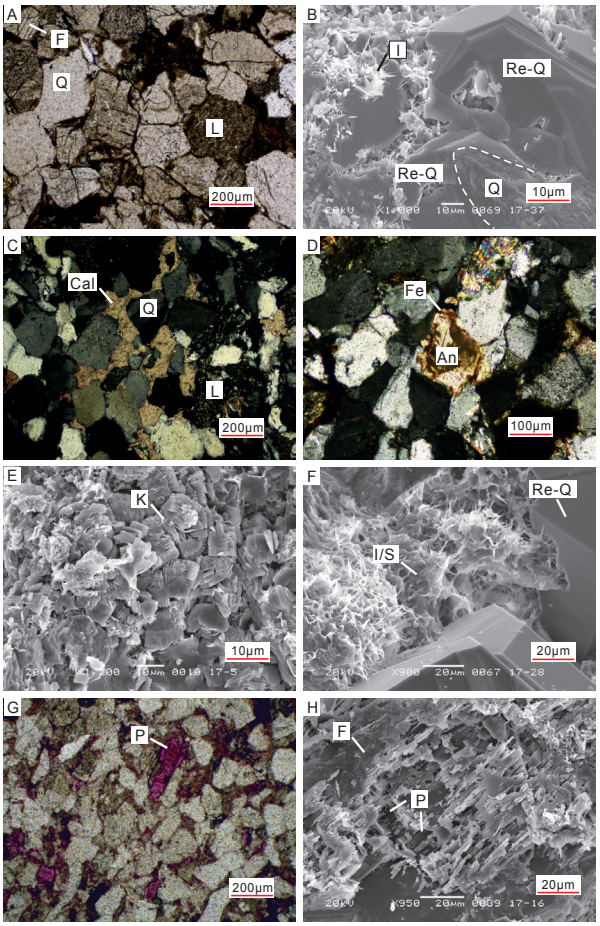

Fig. 7. Photomicrographs showing diagenetic features in the Yanchang Formation sandstones in the study area. (A) Moderately sorted fine- to medium-grained sandstone with sub-angular grains with mainly straight contacts; well W14, C4+5 sub-member, 2395.2 m; Q, quartz; F, feldspar; L, lithic fragment. (B) SEM image showing quartz overgrowths (Re-Q); well W17, C4+5 sub-member, 2480.8 m. (C) Fine- to medium-grained sandstone with prominent calcite cement (Ca); well W14, C4+5 sub-member, 2398.8 m. (D) Ankerite cement (An) with iron-oxide rich margin (Fe); well W3, C6 sub-member, 2493.7 m; (E) SEM photomicrograph showing booklet-like structure of kaolinite (K); well W17, C4+5 sub-member, 2537.4 m; (F) SEM photomicrograph showing illite/smectite mixed-layer clays (I/S) and authigenic quartz cement; well W17, C4+5 sub-member, 2478.7 m; (G) Secondary pore (P) formed as a result of feldspar dissolution; well W14, C4+5 sub-member, 2415.4 m; (H) SEM photomicrograph showing intracrystalline porosity formed as a result of feldspar dissolution; well W17, C4+5 sub-member, 2540.1 m.

resulted in development of overgrowths on quartz grains (Fig. 7B), in turn resulting in significant occlusion of primary porosity.

Within the C4+5 and C6 sandstones in the study area, authigenic cements include calcite together with clay minerals such as chlorite (C4+5 >40%; C6 >50%) and kaolinite (C4+5 > 25%; C6 >20%) with minor illite/smectite (Table 2). Cement precipitation has resulted in significant degradation of intergranular porosity and permeability.

Calcite cements are widespread in the C4+5 and C6 sandstones and include ferrous calcite, ankerite and siderite (Fig. 7C, D; Fig. 8). Microcrystalline and sparry calcite has partly or wholly replaced feldspathic grains (Fig. 7C) and may have been replaced by ankerite (Fig. 7D). Thin sections show calcite cement filling intergranular pore spaces (Figs. 8, 9), resulting in occlusion of the primary porosity. Feldspar dissolution and calcite precipitation occurred preferentially in channel sandstones because of the sandstones' coarser grain size and higher permeability (Fig. 8).

Authigenic chlorite in the C4+5 and C6 sandstones forms rims or coatings which may inhibit the development of quartz overgrowths (c.f. Billault *et al.,* 2003; Aminul, 2009; Berger *et al.,* 2009). Thus primary porosity may locally be preserved by chloritization (cf. Hillier, 1994; Aagaard *et al.,* 2000; Huang *et al.,* 2004; Luo *et al.,* 2009; Huggett *et al.,* 2015).

Kaolinite is formed from the dissolution of feldspar and typically occurs as flat booklets filling pore spaces (Fig. 7E), with an average content of about 26% of the clay minerals present by volume.

Minor illite-smectite mixed-layer clays are also present (Table 2).

Replacement and dissolution

Thin sections from the C6 sub-member sandstones from Well 109 show replacement of quartz and feldspar by calcite (Fig. 8b). Clay minerals (I/S) may replace quartz grains, as evidenced by the presence of grains with irregularly curved margins (Fig. 7F). Replacement processes occur more frequently in channel sandstones which are relatively coarser grained (Worden and Burley, 2003).

Dissolution has created significant local secondary porosity in the Yangchang Formation sandstones. Feldspar grains have undergone dissolution (Fig. 7G), resulting in the formation of inter- and intragranular pore spaces (Fig. 7H). Clay-mineral rich laminae were dissolved producing narrow, elongate dissolution pores (Fig. 9b, c), which were commonly observed in distributary channel and mouth bar sandstones. These elongate pore-spaces may be filled with calcite cement (Fig. 9, b), and hydrocarbon residues may be present where the calcite cement has itself been removed by dissolution (Fig. 9, c).

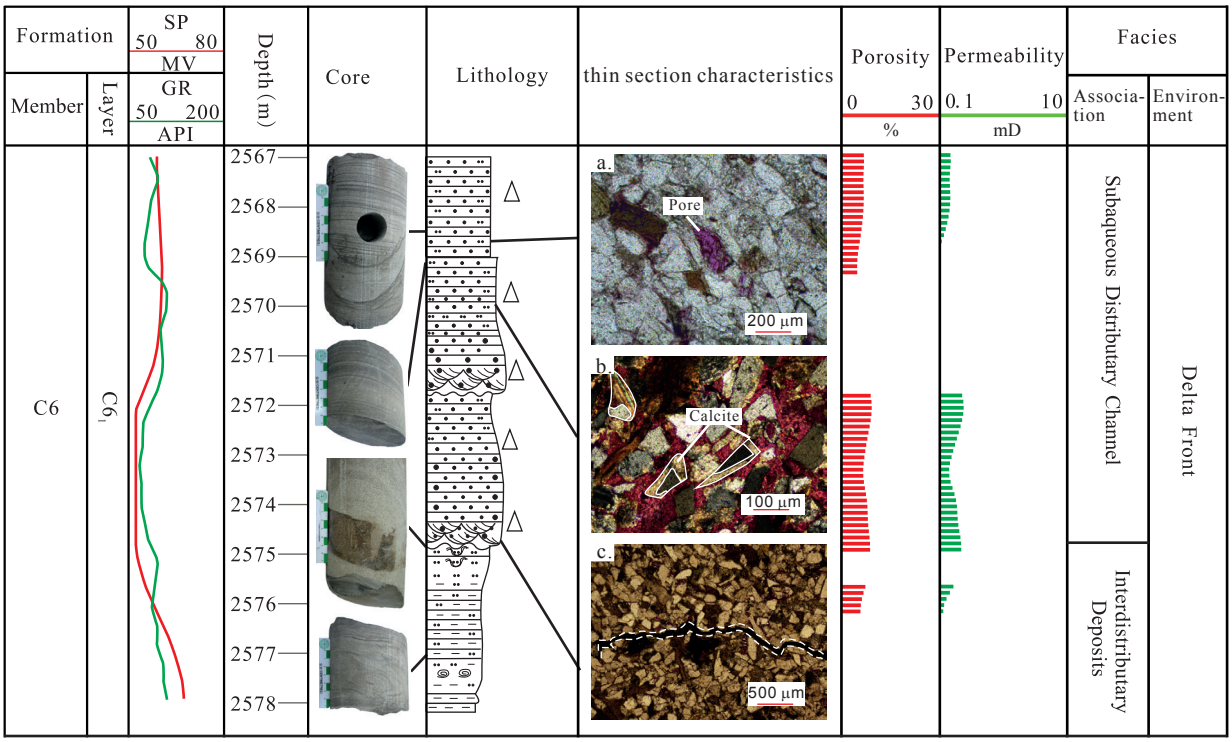

Fig. 8. Sedimentary logs, thin-section characteristics and reservoir properties of C6 sub-member distributary channel sandstones from well W109 (location in Fig. 1). The sandstones have relatively high porosity and permeability. Secondary pores result from calcite dissolution (see thin sections). White triangles indicate samples which fluoresce, indicating minor oil saturation (data from the Huabei Branch Company of SINOPEC).

Calcite dissolution has generated secondary porosity although this process is not extensive in the Yanchang Formation (Zhao *et al.,* 2009). By contrast, dissolution of silicate grains in the Yanchang Formation sandstones is more significant because organic acids which are generated in fresh or brackish water lacustrine settings may generate organic acids which preferentially dissolve aluminum silicate minerals (Surdam *et al.,* 1989). Secondary pores resulting from the dissolution of feldspar and lithic debris make up most of the porosity in the Yangchang Formation sandstones.

Although dissolution can generate significant local porosity, the dissolved materials may be redeposited in the form of cements (e.g. the calcite cements in Fig. 7C), leading to a reduction of porosity and permeability in other parts of the formation.

RESERVOIR PROPERTIES

Although the porosity and permeability of the C4+5 and C6 sandstones are in general low (Table 1), lateral variations in diagenesis have resulted in locally increased values. When the porosity is >8% and the permeability >0.15 mD, reservoir quality was classified as good; it was classified as poor for rocks with porosity <4% and permeability <0.05mD, and moderate when the porosity was 4-8% and permeability 0.05-0.15 mD. There is a positive correlation between permeability (k) and porosity (Φ) (with a correlation coefficient of about 0.7) according to the relationship $k = 0.046\ e^{0.203\Phi}$ on a cross-plot of log permeability versus porosity for the C6 and C4+5 sandstones in the study area (Fig. 10) (n = 309, data provided by the Huabei Branch Company of SINOPEC from eight wells).

In the study area, traces of oil within the sandstones were recorded in cores and thin sections of the C6 interval from wells W109 and W3 (Figs 8 and 9). Oil stains in cores were present in the lower parts of channel sandbodies and in mouth-bar sands. High sandstone porosity and permeability generally correspond to high energy distributary channels and mouth bars (Fig. 9) which therefore have the best reservoir properties.

Progressive diagenesis and cementation also affected the reservoir properties of the C4+5 and C6 sandstones. Early diagenesis resulted in the dissolution of feldspar and carbonate minerals and the development of secondary porosity at depths of less than 2000 m (Luo *et al.*, 2009). However, early diagenetic modification had little impact on reservoir properties (Guo *et al.,* 2008). Subsequent diagenesis occurred during a phase of deep burial during the Cretaceous (97-65 Ma) due to rapid subsidence (Luo *et al*., 2009), resulting in the loss of primary porosity due to compaction and intense cementation. Late-phase diagenesis which occurred during Cenozoic uplift, caused further dissolution (Luo *et al.*, 2009).

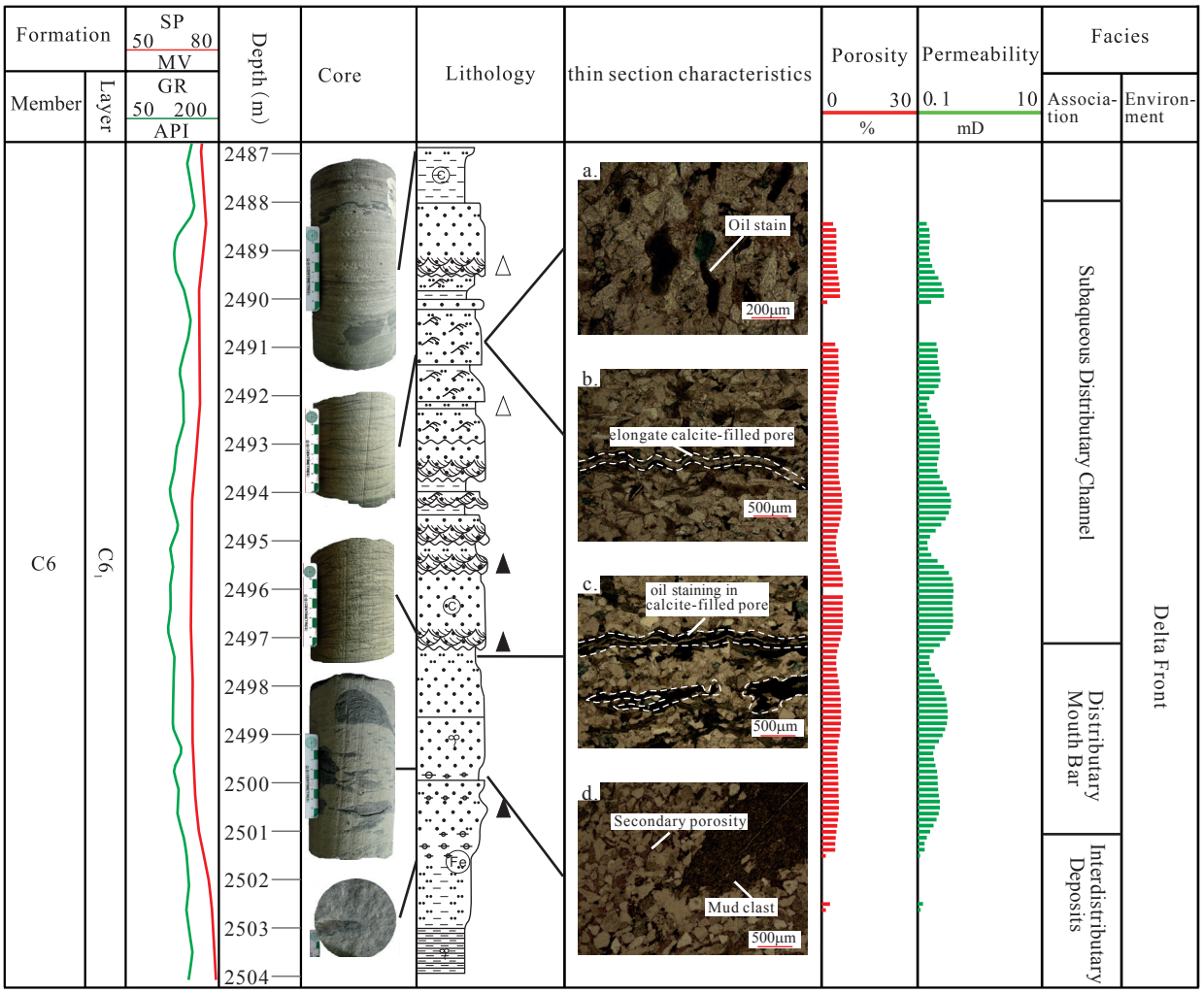

Fig. 9. Sedimenary logs, thin section characteristics and reservoir properties of C6 sub-member mouth bar sandstones from Well W3 (location in Fig. 1). Note that the porosity and permeability of the sandstone were improved by dissolution along clay-mineral rich laminae (thin sections b, c) and feldspathic grains (thin sections a, d). Black triangles indicate samples with visible oil staining; white triangles indicate samples which fluoresce indicating minor oil saturation. Data from the Huabei Branch Company of SINOPEC.

Significant porosity developed during oil emplacement, which retarded cementation by silica-rich and calcite minerals (Luo *et al.,* 2009; Zhao *et al.*, 2009). The effect on permeability is less clear because of the associated overburden compaction. Ferroan calcite and ferroan dolomite cements (Fig. 7C, 7D) were precipitated possibly at the same time as maturation of organic-rich source rocks, and calcite began to replace quartz and feldspar resulting in loss of primary porosity.

Thus, primary porosity in the C4+5 and C6 sandstones was lost during later diagenesis as a result of mechanical compaction and precipitation of quartz and calcite cements. However, some secondary porosity was generated as a result of grain dissolution.

CONCLUSIONS

This paper has described the sedimentary characteristics of deep-water lacustrine delta-front sandstones in the C4+5 and C6 sub-members of the Upper Triassic Yanchang Formation in a study area in the western Ordos Basin. Facies interpretations from well logs and other data suggest that, in response to the relatively deep-water setting, the lacustrine delta had a broad delta front and narrow delta plain. Sandstones deposited in the delta front consist of relatively fine-grained mud-rich deposits.

In contrast to shallow-water deltaic reservoirs, the deep-water delta-front deposits including distributary channel and mouth bar sandstones have relatively poor reservoir properties. These sandstones were subjected to mechanical compaction and diagenesis during burial. Intense mechanical compaction and precipitation of quartz and calcite cements resulted in low permeability and relatively low primary porosities. However some secondary porosity was created during late-phase dissolution, and delta-front sandstones in the Yanchang Formation may therefore have local reservoir potential.

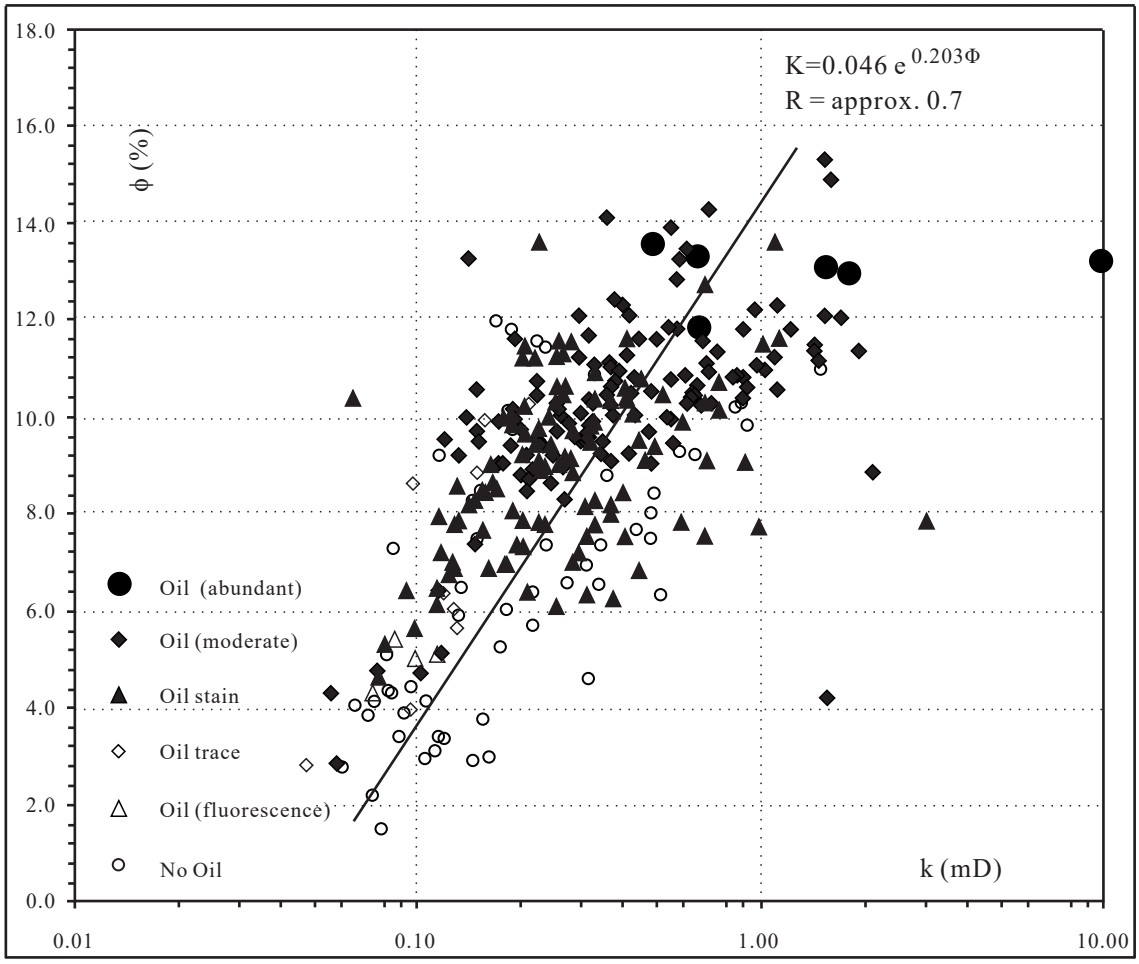

Fig. 10. Cross-plot of porosity versus log permeability for the C6 and C4+5 sandstones from wells W2, W3, W4, W5, W14, W17, W103 and W109 (locations in Fig. 1) showing that the sandstones in general have low porosity (<2-15%) and permeability (<0.1 - 10 mD) (Table 2). There is a positive correlation between porosity and permeability with a correlation coefficient of about 0.7. Oil-saturated sandstones had porosity and permeability greater than 12.5% and 0.45 mD respectively. Data derived from the analysis of 309 core samples from the eight wells listed above at depths of 2180–2650 m (Huabei Branch Company of SINOPEC).

ACKNOWLEDGEMENTS

This study was partly supported by the National Natural Science Foundation of China (grants no. 41572080 and 41272132). The first author thanks the Exploration and Development Research Institute, Huabei Branch Company of SINOPEC in Zhengzhou, China, for geological data and support. Zhao Shu of SINOPEC assisted with the core descriptions and provided useful suggestions. The comments of three anonymous referees on earlier versions of the manuscript are acknowledged with thanks and resulted in improvement of the presentation.

REFERENCES

AAGAARD, P., JAHREN, J.S., HARSTAD, A.O., NILSEN, O. and RAMM, M., 2000. Formation of grain coating chlorite in sandstones: Laboratory synthesized vs. natural occurrences. *Clay Minerals*, **35**(1), 261-269.

AMINUL, I. M., 2009. Diagenesis and reservoir quality of Bhuban sandstones (Neogene), Titas Gas Field, Bengal Basin, Bangladesh. *Journal of Asian Earth Sciences,* **35**(1), 89-100.

BERGER, A., GRIER, S. and KROIS, P., 2009. Porosity-preserving chlorite cements in shallow-marine volcaniclastic sandstones: Evidence from Cretaceous sandstones of the Sawan gas field, Pakistan. *AAPG Bull.,* **93**(5), 595-615.

BILLAULT, V., BEUTORT, D., BARONNET, A., and LACHARPAGNE, J. C., 2003. A nanopetrogrphic and textural study of grain-coating chlorites in sandstone reservoirs. *Clay Minerals,* **38**(3), 315-328.

COLEMAN, J. M. (Ed.), 1982. Deltas: Processes of deposition and models for exploration (Second Edition): Boston, International Human Resources Development Corporation, 124 p.

DARBY, B.J, and RITTS, B.D., 2002. Mesozoic contractional deformation in the middle of the Asian tectonic collage: the intraplate Western Ordos fold–thrust belt, China. *Earth & Planetary Science Letters*, **205**(02), 13-24.

DU, G.C., 2014. Sedimentary facies and sedimentary model for the Chang 6_2 oil measures of the Triassic Yanchang Formation in the Qilicun Oil Field, Ordos Basin. *Sedimentary Geology and Tethyan Geology,* **34**(4), 30-39 (in Chinese with English abstract).

GUO, Y.R., LIU, H.Q, LI, X.B., WANYAN R., and ZHENG, X.M., 2008. Method System on Studying Sequence Stratigraphic Framework of Large Sagged Lacustrine Basin: a case study from Mesozoic Yanchang Formation, Ordos Basin. *Acta*

Sedimentologica Sinica, **26**(3), 384-391(in Chinese with English abstract).

HAN, Y. L., WANG, C. Y. WANG, H. H., LI, S. C., ZHENG, R. C., WANG., C.Y. and LIAO, Y., 2009. Sedimentary Characteristics of Shallow-water Deltas in the Chang 8 Subsection of Yanchang Formation, Jiyuan area. *Acta Sedimentologica Sinica*, **27**(6), 1057–1064 (in Chinese with English abstract).

HANSON, A.D., RITTS, B. D. and MOLDOWAN, J. M., 2007. Organic geochemistry of oil and source rock strata of the Ordos Basin, north-central China. *AAPG Bulletin,* **91**,1273-1293.

HILLIER, S., 1994. Pore-lining chlorites in siliciclastic reservoir sandstones: Electron microprobe, SEM and XRD data, and implications for their origin. *Clay Minerals,* **29**(4), 665-679.

HU, J.M, LIU, X.S. and LI, Z.H., 2013. SHRIMP U-Pb zircon dating of the Ordos Basin basement and its tectonic significance. [J] *Science Bulletin*, **58**(1), 118-127.

HUANG, S.J., XIE, L.W., ZHANG, M., WU, W.H., SHEN, L.C. and LIU, J., 2004. Formation mechanism of authigenic chlorite and relation to preservation of porosity in non-marine Triassic reservoir sandstones, Ordos Basin and Sichuan Basin, China. *Journal of Chengdu University of Technology (Science & Technology Edition)*, **31**(3), 273-281 (in Chinese with English abstract).

HUGGETT, J. M., BURLEY, S. D., LONGSTAFFE, F. J., SAHA, S. and OATES, M., 2015. The nature and origin of authigenic chlorite and related cements in Oligo-Miocene reservoir sandstones, Tapti gas fields, Surat depession, offshore Western India. J*ournal of Petroleum Geology,* **38**(4), 383-410.

JOHNSON, E. A., SHU, L. and ZHANG, Y.L., 1989. Depositional environments and tectonic controls on the coal-bearing Lower to Middle Jurassic Yan'an Formation, southern Ordos Basin, China. *Geology*, **17,** 1123 - 1126.

KASSE, C, 2014. Fluvial response to rapid high-amplitude lake-level changes during the Late Weichselian and early Holocene, Ain River valley, Jura, France. *Boreas,* **43**(2), 403-421.

KORUS, J.T. and FIELDING, C.R., 2015. Asymmetry in Holocene river deltas: Patterns, controls, and stratigraphic effects. *Earth-Science Reviews*, **150**, 219-242.

LEI, Z.Y. and ZHANG, C. J., 1998. Study of petroleum system in Ordos Basin. *Petroleum Explorationist*, **3**(1), 11-15 (in Chinese with English abstract).

LI, S. L., ZHAO S., FU J., QING, B.C., and LIU, L.W., 2008. Adopting the distribution and evolution laws of depositional microfacies in analyzing the directions of oilfield development in the Zhenjing oilfield, Ordos basin. *Earth Science Frontiers,* **15**(1), 85-93 (in Chinese with English abstract).

LI, X.B., LIU, H.Q., WANYAN, R., WEI, L.H. , LIAO, J.B., FENG, M., MA, Y.H. and BAI, Y.L, 2009. Tectonic Evolution of the Tianhuan Depression and the Western Margin of the Late Triassic Ordos. *Acta Geologica Sinica – English Edition*, **83**(6), 1136-1147.

LIN, H.B., HOU, M.C., CHEN, H.D., and DONG, G.Y., 2008. Characteristics and evolution of the sedimentary system of Upper Triassic Yanchang Formation in Ordos Basin, China. *Journal of Chengdu University of Technology (Science & Technology Edition),* **35**(6), 674-680 (in Chinese with English abstract).

LIU, S., ZHU, X., WANG, R. and JIN, T., 2012. Study on Sedimentary System of Shallow Delta in Continental Lake Basin. *Journal of Shandong University of Science and Technology*, **31**(5), 93 – 104 (in Chinese with English abstract).

LUO, J.L., LIU, X.H., LIN, T., ZHANG, S. and LI, B., 2006. Impact of diagenesis and hydrocarbon emplacement on sandstone reservoir quality of the Yanchang Formation (Upper Triassic) in the Ordos basin. *Acta Geologica Sinica*, **80**(5), 664-673 (in Chinese with English abstract)

LUO, J. L., S. MORAD, A. SALEM, J. M. KETZER, X. L. LEI, D. Y. GUO and O. HLAL, 2009. Impact of diagenesis on reservoir-quality evolution in fluvial and lacustrine-deltaic sandstones: evidence from Jurassic and Triassic sandstones from the Ordos Basin, China. *Journal of Petroleum Geology,* **32**, 79-102.

MA, Y.Z., SETO, A. and GOMEZ, E., 2009. Depositional facies analysis and modelling of Judy Creek reef complex of the Late Devonian Swan Hills, Alberta, Canada. *AAPG Bulletin* **93**(9), 1235-1256.

SHOU, J.F., ZHU, G.H. and ZHANG, H.L., 2003. Lateral structure compression and its influence on sandstone diagenesis -- a case study from the Traim Basin. A*cta Sedimentologica Sinica*, **21(**1), 90-95 (in Chinese with English abstract).

SLATT, R.M., 2006. Stratigraphic reservoir characterization for petroleum geologists, geophysicists and engineers. Handbook of petroleum exploration and production **6.** University of Oklahoma, Norman, Oklahoma 73019. USA.

SURDAM, R.C., CROSSEY, L.J., HAGEN, E.S. and HEASLER, H.P., 1989. Organic-inorganic interactions and sandstone diagenesis. *AAPG Bulletin* **73**(1), 1-23.

WANG, F., TIAN, J.C., FAN, L.Y., CHEN, R. and QIU, J.L., 2010. Evolution of Sedimentary Fillings in Triassic Yanchang Formation and its Response to Indosinian Movement in Ordos Basin. *Natural Gas Geoscience,* **21**(6), 882-889 (in Chinese with English abstract) .

WANG, B.Q. and AL-AASM, I.S., 2002. Karst-controlled diagenesis and reservoir development: example from the Ordovician main-reservoir carbonate rocks on the eastern margin of the Ordos basin, China. *AAPG Bulletin,* **86**, 1639-1658.

WANG, J.F., ZHAO, W.Z., GUO, Y.R. and ZHANG, Y. L., 2010. Analyses of Petroleum Resources Status and Exploration Potentialities, Yanchang Formation of Triassic in Ordos Basin. *Geoscience*, **24**(5), 957-964 (in Chinese with English abstract).

WANG, J.F., GUO, Y.R., ZHANG, Y.L., LIU, H.W. and MA, D.B., 2009. Sequence stratigraphic framework and sedimentary facies of Yanchang Formation, Triassic system in Ordos basin. *Geoscience*, **23**(5), 803-808 (in Chinese with English abstract).

WANG, X.J., WANG, Z.X., LIU, X.Y., and ZENG, J.H., 2008. Restoring palaeo-depth of the Ordos basin by using uranium response from Gr logging. *Natural Gas Industry,* **28**(7), 46-48 (in Chinese with English abstract).

WEI, B., WEI, H.H., CHEN, Q.H. and ZHAO, H., 2003. Sediment provenance analysis of Yanchang Formation in Ordos Basin. *Journal of Northwest University(Natural Science Edition),* **33**(4), 447-450 (in Chinese with English abstract).

WORDEN, R.H. and BURLEY, S., 2003. Sandstone diagenesis: the evolution of sand to stone. In: Sandstone Diagenesis: Recent and Ancient. Burley S. and Worden, R. H. (Eds), Blackwells, 1-44.

WU, F.L., LI, W.H., LI, Y.H. and XI, S. L., 2004. Delta sediments and evolution of the Yanchang Formation of Upper Triassic in Ordos Basin. *Journal of Palaeogeography,* **6**(3), 307-315 (in Chinese with English abstract).

XIAO, J. L., FAN, J.W., ZHOU, L., ZHAI, D.Y., WEN, R.L. and QIN, X.G., 2013. A model for linking grain-size component to lake level status of a modern clastic lake. *Sedimentary Geology,* **69,** 149-158.

XIE, X. and HELLER, P. L., 2013. U–Pb detrital zircon geochronology and its implications: The early Late Triassic Yanchang Formation, south Ordos Basin, China. *Journal of Asian Earth Sciences,* **64**, 86-98.

YAO, G.Q., MA, Z., ZHAO, Y.C. and WANG, X.Y., 1995. Reservoir characteristics of distributary channel sand bodies of shallow water delta. *Acta Petrolei Sinica*, **16(**1), 24 – 31 (in Chinese with English abstract).

YANG, M.H., LIU, C.Y., ZHENG, M.L., LAN, C.L. and TANG, X., 2007. Sequence framework of two different kinds of margins and their response to tectonic activity during the Middle-Late Triassic, Ordos Basin. *Science In China Series D – Earth Sciences*, **50**, 203-216.

YANG, Y.T., LI, W. and MA, L., 2005. Tectonic and stratigraphic controls of hydrocarbon systems in the Ordos basin: A multicycle cratonic basin in central China. *AAPG Bulletin,* **89,** 255 - 269.

YANG, H., LIU, Z.L., ZHU, X.M., DENG, X.Q., ZHANG, Z.Y., and QI, Y.L., 2013. Provenance and depositional systems of the Upper Triassic Yanchang Formation in the southwestern Ordos Basin, China. *Earth Science Frontiers*, **20**(2), 10-18 (in Chinese with English abstract).

YU, Y., DAI, S., YIN, T., MAO, P., and DONG, L., 2009. Study on shallow-water delta deposition in Yanchang Formation of Xiasiwan, Ordos Basin. *Special Oil and Gas Reservoirs*, **16**(5), 28 – 31 (in Chinese with English abstract).

YUAN, X.J., LIN, S.H., LIU, Q., YAO, J.L., WANG, L., GUO, H., DENG, X.Q. and CHENG D.W., 2015. Lacustrine fine-grained sedimentary features and organic-rich shale distribution pattern: A case study of Chang 7 Member of Triassic Yanchang Formation in Ordos Basin, NW China. *Petroleum Exploration and Development,* **42**(1), 34-43 (in Chinese with English abstract).

YUE, Q.Z, MERCIER, J.L, and VERGELY, P., 1998. Extension in the rift systems around the Ordos (China), and its contribution to the extrusion tectonics of south China with respect to Gobi–Mongolia. *Tectonophysics*, **285**(1), 41-75.

ZENG, L.B. and LI, X.Y., 2009. Fractures in sandstone reservoirs with ultra-low permeability: A case study of the Upper Triassic Yanchang Formation, Ordos Basin, China. *AAPG Bulletin*, **93**, 461-477.

ZHAO, J. X., HUANG, D. C., LUO, , Y., LU, Q. and ZHU, P., 2009. Diagenetic features of reservoirs in the Chang-6 member, south Ordos basin. *Natural Gas Industry*, **29** (3), 1-4 (in Chinese with English abstract)

ZHAO, W. Z., WANG, H. J., YUAN, X. J., WANG, Z.C. and ZHU, G.Y., 2010. Petroleum systems of Chinese non-marine basins. *Basin Research*, **22,** 4–16.

ZHENG, H.R., 2012. New advances in petroleum geology and exploration techniques of clastic reservoirs in the four large-sized basins in central-western China. *Oil &Gas Geology*, **33**(4), 497 -505 (in Chinese with English abstract).

ZHU, W. L., LI, J.P., ZHOU, X. H. and GUO, Y. H., 2008. Neogene shallow water deltaic system and large hydrocarbon accumulations in Bohai Bay, China. *Acta Sedimentologica Sinica*, **26**(4), 575 -582 (in Chinese with English abstract).

ZHU, R.K. and TAO, S.Z., 2008. Formation and distribution of shallow-water deltas and central-basin sand bodies in large open depression lake basins. *Acta Geologica Sinica*, **82**(6), 813 - 825 (in Chinese with English abstract).

ZHU, X.M., PAN, R., ZHAO, D.N., LIU, F, WU, D., LI, Y. and WANG, R., 2013. Formation and development of shallow-water deltas in lacustrine basin and typical case analyses. *Journal of China University of Petroleum*, **37**(5), 7-14 (in Chinese with English abstract).

ZOU, C.N., ZHAO, W.Z., ZHANG, X.Y., LUO, P., WANG, L., LIU, L.H., XU, E S.H., YUAN, X.J., ZHU, R.K. and TAO, S. Z., 2008. Formation and distribution of shallow-water deltas and central-basin sand bodies in large open depression lake basins. *Acta Geologica Sinica*, **82**(6), 813-825 (in Chinese with English abstract).